

Microwave response and electrical transport studies of disordered s wave superconductor: NbN thin films

D. Hazra, S. Jebari, R. Albert, F. Blanchet, A. Grimm, C. Chapelier and M. Hofheinz
Univ. Grenoble Alpes, CEA, INAC-PHELIQS, 38000 Grenoble, France

It is now well known that the properties of the disordered s wave superconductors can deviate significantly from the prediction of standard Bardeen-Cooper-Schrieffer (BCS) theory. By measuring the temperature dependence of the resonance frequency, f_0 , of microwave resonators made from disordered NbTiN and TiN thin films, at low temperatures, below half of the superconducting critical temperature, T_c , Driessen et al. [1] demonstrated that f_0 vanishes faster than predicted from the BCS theory. Here, we report on the temperature dependence of f_0 of microwave resonators made from disordered NbN thin films at higher temperatures— typically from 0.4 to $0.8T_c$. In this temperature range, we demonstrate that f_0 vanishes slower than predicted from the BCS theory. We discuss the possible role of electronic inhomogeneity and possibility of appearing a pseudogap-like feature. We also discuss the possibility of a faster downturn of the superfluid density, n_s , near T_c , resembling a Berezinski-Kosterlitz-Thouless (BKT) type transition.

I. INTRODUCTION

It had been a long-standing paradigm that the superconducting properties are unaffected by disorder as long as the time reversal symmetry is intact [2]. Consequently, it is expected that T_c of an s-wave superconductor would be related to its energy gap, Δ , by BCS relation, irrespective of its normal state resistivity. But in last few decades, theory and numerical simulations, followed by several experiments, have demonstrated that even for a moderate level of disorder there can be a significant departure from standard BCS like behaviour [3–13].

Followed by these early developments, in recent times, there has been again a resurgence to study the properties of disordered superconductors and already a large wealth of physics has been unearthed — which are not conceivable by conventional BCS theory — like, superconductor-insulator transition [5, 9], magnetic flux quantization in disordered driven insulating film [14], finite superfluid stiffness above T_c [15], spatially inhomogeneous superconductivity [16–18], jump in superfluid density near T_c [19], strong phase fluctuation [20] and localization of the preformed Cooper pairs [21], to mention only few.

Most of these studies, however, focus on scanning tunnelling spectroscopy (STS) or magnetoresistance measurements. In comparison to that, probing disordered superconductors using microwave signal has been a few (see e.g, [1, 15, 22–24]). Moreover, recently, the microwave resonators made of disordered superconductors have been explored to perform circuit quantum electrodynamics (circuit-QED) experiments at a high magnetic field for quantum computation and also as high impedance resonators [25–29]— thanks to their high kinetic inductance. These, in turn, demand to probe the disordered superconductors using the microwave as their detailed properties might impact circuit-QED experiment’s outcome.

Here, we report on the microwave response of disordered s wave superconductors: NbN thin films. For that, microwave resonators are fabricated and their resonance frequencies, f_0 , are measured as a function of temper-

ature. With increasing disorder, we observe a systematic departure from BCS behaviour: f_0 extrapolates to zero, in the BCS framework, at a temperature T_c which is always higher than T_{c1} where resistivity goes to zero. Moreover, the difference, $T_c - T_{c1}$, widens with disorder. We discuss whether the observed behaviour can be due to the electronic inhomogeneity or the presence of a pseudogap-like feature. We also analyze if a sudden downturn of the superfluid density, n_s , near T_c , resembling a BKT type transition, is behind the observed microwave response of the samples.

II. EXPERIMENTS, RESULTS AND ANALYSIS

Three NbN thin-films are deposited by d.c magnetron sputtering of an Nb target, in the atmosphere of nitrogen and argon gas mixture, onto oxide-coated Si substrate at room temperature. Prior to NbN deposition, the substrates are cleaned by back-sputtering and a 20 nm MgO buffer layer is added to improve the film quality. Microwave resonators, transmission lines and Hall bars are fabricated using standard optical lithography and reactive ion etching technique. The detailed fabrication processes are reported elsewhere [30, 31]. The electrical transport and microwave transmission (S_{21}) measurements are performed down to liquid helium temperature.

In Fig.1, we show the temperature variation of resistance for all three films near T_c . The resistances are normalized with respect to maximum values of the respective sample. The room temperature sheet resistance, R_{\square} , the thicknesses, d , and the Ioffe-Regel parameter, $k_F\ell$, are summarized in Table-I. The temperatures T_{c1} s, where resistances go to zero, are also listed in Table-I. $k_F\ell$ are determined from the electrical resistivity, ρ_{xx} , and Hall coefficient, R_H , at room temperature (see Appendix for thickness and $k_F\ell$ determination). The $k_F\ell$ values indicate that our films are in the strongly disordered limit [32].

To probe the microwave response of the samples, five

TABLE I. Summary of the various parameters. See the main text for details.

Samples	R_{\square} (Ω)	d (nm)	$k_F \ell$	T_{c1} (K)	T_c (K)	$T_c - T_{c1}$ (K)
S1	1100	~ 3.5	~ 1.7	7.85	9.37	1.52
S2	540	~ 5.0	~ 2.5	9.19	10.20	1.01
S3	160	10.0	4.1	11.35	12.02	0.67

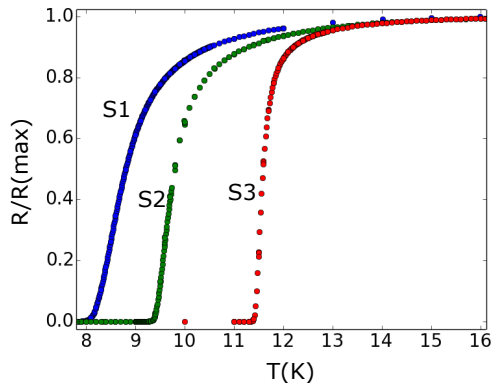


FIG. 1. Resistance, R , as a function of temperature, T , near superconducting transition for three NbN thin films we have studied. The resistances are normalized by the maximum resistance of the respective film. The transition temperatures, T_{c1} s, where R become zero, are listed in Table-I.

identical quasi-lumped-element microwave resonators are fabricated from each film. These resonators are coupled to a 50Ω matched transmission line (TL) with varying coupling capacitances, as shown schematically in Fig.2a, to probe the microwave response through the transmission, S_{21} , measurement. We also show a simplistic schematic diagram of our experimental setup. In Fig.2b, we show optical micrograph image of a resonator, coupling capacitor, and part of the TL. For all three samples, the central conductor of the TL is fabricated from 300 nm thick NbN layer. Our lumped-element resonators are meander-shaped with a linewidth of $2 \mu\text{m}$. A zoomed-in portion of the resonator is shown in the right-bottom of Fig.2b. The coupling capacitance is provided by sandwiching a Si_3N_4 layer between the central conductor of the TL and a top electrode connecting the resonator, as shown in Fig.2b.

In Fig.3, we plot $|S_{21}|$ for S1 at $T = 4.2$ K. As expected, we observe five fundamental resonances (dips) corresponding to five different coupling capacitors: the lowest f_0 corresponds to the highest capacitance and vice-versa. A magnified version of the resonance dip, that corresponds to the lowest f_0 , is shown in the inset. The f_0 is extracted from fitting the resonance curve with the following equation [33]:

$$S_{21} = \frac{1 + 2iQ_i \frac{\Delta f_0}{f_0}}{1 + 2iQ_i \frac{\Delta f_0}{f_0} + \frac{Q_i}{Q_c}}, \quad (1)$$

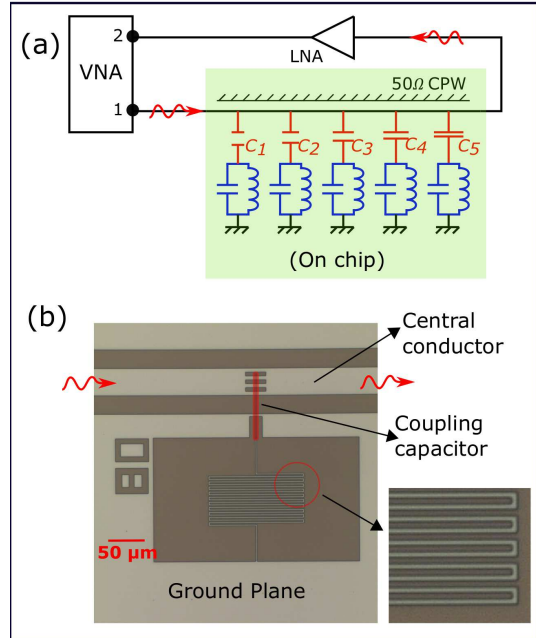


FIG. 2. (a) A schematic of our microwave transmission measurement. Five identical microwave resonators are side coupled capacitively to a 50Ω matched transmission line with different capacitances. Here, LNA and VNA stand for low noise amplifier and vector network analyzer, respectively. (b) An optical micrograph image of a resonator and a part of the transmission line. The coupling capacitor is shown by a false red-colour. The resonator is meander-shaped with linewidth $2 \mu\text{m}$. A zoomed-in portion of the resonator is shown in the right-bottom of Fig.b.

here, Q_i and Q_c are internal and coupling quality factor, respectively, and $\Delta f_0 = f - f_0$.

To study the temperature dependence of f_0 , the first four resonance dips of each sample are traced as a function of temperature. In the limit $L_k \gg L_g$, where, L_k is the kinetic and L_g is the geometric inductance of the resonator, f_0 can be expressed, in terms magnetic penetration depth λ , as (see Appendix for detail)

$$\frac{f_0(T)}{f_0(0)} = \frac{\lambda(0)}{\lambda(T)}, \quad (2)$$

here, $f_0(0)$ is the resonance frequency at $T = 0$.

In the dirty limit — i.e, $\ell \ll \xi$, where ℓ is elastic mean free path ~ 0.5 nm and ξ is the coherence length ~ 5 nm for our samples as measured from Hall measurement

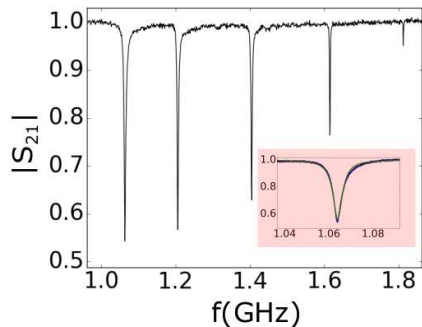


FIG. 3. Microwave transmission, $|S_{21}|$, data of S1 at 4.2 K. Five dips correspond to the different coupling capacitances, C_c . The inset shows the zoomed-in version of the dip corresponding to the lowest f_0 . The solid line is a fit with Eq.1

and magnetoresistance data near T_c — the BCS theory results [34]

$$\frac{\lambda(T)}{\lambda(0)} = \frac{1}{\sqrt{\delta(T) \tanh\left(\beta\delta(T)\frac{T_c}{T}\right)}} \quad (3)$$

, here, $\delta(T) = \Delta(T)/\Delta(0)$ is normalized energy gap and $\beta = \Delta(0)/2k_B T_c$.

Combining Eq.2 and Eq.3 yields

$$f_0(T) = f_0(0) \sqrt{\delta(T) \tanh\left(\beta\delta(T)\frac{T_c}{T}\right)}. \quad (4)$$

To verify the agreement between Eq.4 and our experimental data, we show the temperature dependence of f_0 for all three samples in Fig.4. In the same figure, we also plot the temperature dependence of resistance near T_c , for comparison. The solid lines are fit with Eq. 4, where, for the temperature dependence of δ , we have simulated it using BCS theory. $f_0(0)$ and T_c are taken as fit parameters. The T_c , as extracted from the fit, are listed in Table-I. We see that T_c , for all three samples, differ significantly from T_{c1} where resistance is zero. In other words, f_0 and resistance vanish at different temperatures, T_c and T_{c1} , respectively. Moreover, the temperature region $T_c - T_{c1}$, shown by shaded area, systematically increases with disorder (see Table-I).

Here, we would like to mention two important points. Firstly, to fit with Eq.4, if we set $T_c = T_{c1}$ and take $f_0(0)$ as the sole fitting parameter, we see that no meaningful fit is possible, especially for S1 and S2. Secondly, for $\beta (= \Delta(0)/2k_B T_c)$, we have chosen $\beta = 1.1$ for all three samples. Though, we have not experimentally determined the $\Delta(0)$ for the reported samples, tunnelling

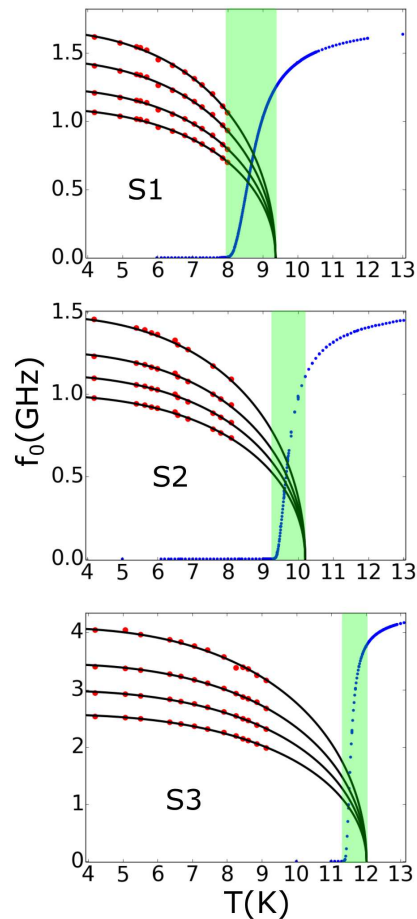


FIG. 4. Experimentally obtained resonance frequency (the red dots), f_0 , as a function of temperature. The solid lines are fits with Eq.4. The temperatures, T_c s, where f_0 go to zero, are listed in Table-I. We also plot the temperature variation of resistance (the blue dots).

experiments on NbN/MgO/NbN tunnel junction resulted in $\beta = 1.1$ for similar kinds of films we deposited [30, 31]. This number is consistent with Reference [20, 35] for sputtered deposited NbN films with similar T_c s. Further, STS measurement on a film identical to S3 resulted $\beta = 1.1$ (see Appendix). Here, we would like to point out that for disordered superconductors like ours, a spatially inhomogeneous superconducting state may be developed [16, 17, 22]. In that case, β refers to a spatially averaged parameter.

III. DISCUSSION

To understand the observed behaviour of Fig.4, first, we concentrate on the least disordered sample, S3. We note that f_0 , in the BCS framework, mimics energy gap parameter δ via Eq.4. Thus, at the first instance, it appears that there exists a region, shown by the shaded

area, where the global superconductivity is destroyed, as evident from the existence of a finite resistance, but exists finite 'average gap'— the pseudogap. To verify this, we perform STS measurement on a film identical to S3, deposited under the identical condition that resulted in exactly the same T_c as S3. We didn't observe any pseudogap or spatial inhomogeneity in this film (see Appendix). Here, we would like to point out that several groups have probed disordered NbN films by STS studies. No pseudogap was observed, with best of our knowledge, for films with $T_c < 6.5K$ [18, 20, 36]. Therefore, it is unlikely that S3, with $T_c \sim 11.5K$, possesses any pseudogap-like features.

To explore the other possible explanation for the observed behaviour of Fig.4, we note that f_0 is related to δ via λ . Thus, if λ deviates from the BCS temperature variation (Eq.3) and $1/\lambda$ does have a faster downturn near T_c , the temperature variation of f_0 for S3 is explainable. Such an observation, indeed, was made for both 2D and 3D disordered NbN films in direct λ measurement [19, 20, 37] and was associated, for 2d films, with a BKT type transition that predicts a jump in superfluid density, $n_s (\propto 1/\lambda^2 \propto f_0^2)$, at a temperature T_{BKT} before T_c . Here, we should point out that in the above references the authors also observed additional smearing, in the temperature dependence of $1/\lambda^2$, which they attributed to the vortex core energy [38, 39].

For S1 and S2, since they are thinner than S3 and more disordered, a faster downturn of n_s near T_c are more probable [19, 20, 37–39]. However, for S1, we note that f_0 is still finite at T_{c1} . Thus, in this case, a mere downturn of n_s near T_c is not sufficient to explain our experimental data. Since we didn't perform any STS experiment on films identical to S1 and S2, we cannot completely rule out the possibility of a pseudogap-like features in S1 and S2. Thus, for S1 and S2, particularly for S1, it is possible that both a pseudogap-like feature as well as a downturn of n_s are responsible for the observed behaviour of Fig.4. However, a further experimental probe near T_c , by STS and direct λ measurements, is required to have a final conclusion on that.

Finally, we would like to mention that Driessen et al.[1] reported temperature dependent f_0 in disordered NbTiN and TiN thin films. With increasing disorder, like us, they also observed a systematic departure from BCS behaviour. However, they observed that f_0 extrapolates to zero in BCS framework at a temperature lower than where resistance goes to zero (i.e, $T_{c1} > T_c$), which is clearly in contradiction to our observation. The main reason behind this apparent contradiction is, in their study, Driessen et al. restricted themselves to very low temperatures, typically below $0.35 T_c$. In that temperature range, using a 3 dimensional model of pair-breaking mechanism, they argued that a modification in the quasiparticle density of state, due to disorder-induced electronic inhomogeneity, is responsible for the observed departure from BCS behaviour. In our case, on the contrary, we explore the temperature range above $0.4 T_c$. Moreover, our films

are in the 2-dimensional limit. In our case, therefore, it is possible that BKT like transition dominates over the effect due to the possible modification of the quasiparticle density of state.

IV. SUMMARY AND CONCLUSION

In summary, we have probed disordered s wave superconductor, three NbN thin films, with Ioffe-Regel parameters, $k_F \ell < 4.1$, by electrical transport and microwave signal. Microwave resonators are fabricated and temperature dependence of their resonance frequency, f_0 , is traced in the superconducting state at temperatures above $0.4T_c$. For our measured films, f_0 extrapolates to zero, in the BCS framework, at a temperature T_c which is always higher than T_{c1} where resistivity goes to zero. To explain our experimental observation, we discuss the possibility of a pseudogap-like feature as well as the possibility of a faster downturn, than that is expected from the BCS theory, of the temperature dependence of n_s near T_c . We, however, advocate for further experiments, near T_c , to have a final conclusion.

V. ACKNOWLEDGEMENTS

We acknowledge financial support from the French National Research Agency, Grant No. ANR-14-CE26-0007WASI and Grant No. ANR-16-CE30-0019-ELODIS2, from the Grenoble Fondation Nanosciences, Grant JoQOLaT; and from the European Research Council under the European Unions Seventh Framework Programme (FP7/2007-2013), ERC Grant Agreement No. 278203WiQOJo.

VI. APPENDIX

A. Thin film characterization

We have deposited a series of NbN thin-films of thicknesses in the range $300 < d < 10$ nm. The electrical resistivity and Hall measurements are performed on all the films. For microwave transmission measurements, the resonators are fabricated on the three thinnest films where $L_k \gg L_g$ and f_0 can be expressed in the normalized form of Eq.4.

The thicknesses, d , of the thicker films, $d \geq 10$ nm, are first estimated from optimized deposition rate and then confirmed by the cross-sectional image of high resolution scanning electron micrograph. For some films, the thicknesses are reconfirmed by profilometry measurement. In this way, we could determine film thickness within 10 to 15 % accuracy.

The electron density, n , for the thicker films are determined from the Hall coefficient, R_H , at room temperature, using the formula: $R_H = 1/ne$, here, e is the charge

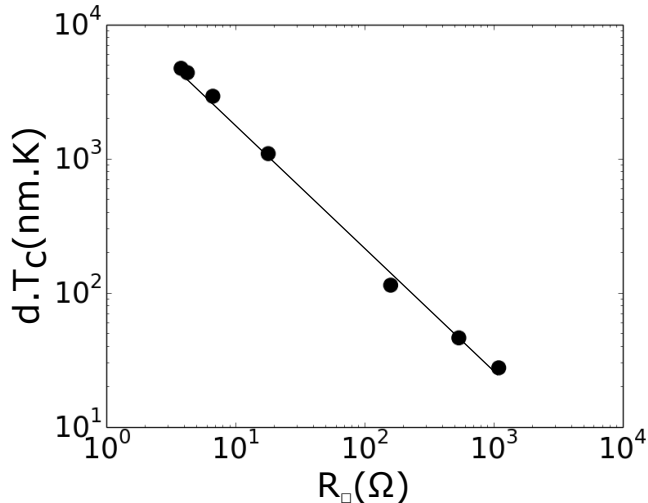


FIG. A1. Variation of $d.T_c$ with square resistance R_{\square} in log scale. The solid line is a straight line fit.

of the electron. The $k_F \ell$ s are determined from the following formula [40], assuming free electron model:

$$k_F \ell = \frac{\hbar(3\pi^2)^{2/3}}{n^{1/3} \rho e^2}. \quad (\text{A1})$$

Here, ρ is the longitudinal electrical resistivity and \hbar is the reduced Planck constant.

To estimate the thicknesses of the thinner films, S1 and S2, we follow two methods:

(1) We note that, for identical deposition condition, n does not change significantly with d . This observation is consistent with reference [35]. For our films with known d , from Hall measurements at room temperature, we estimate $n \sim 2.0 \times 10^{29}/\text{m}^3$. This, in combination with the slope of the Hall resistance ($= 1/ned$), is used to estimate the thicknesses of S1 and S2.

(2) Our films with known thicknesses follow the scaling law, recently proposed by Yachin et al. [41]:

$$d.T_c = A.R_{\square}^{-B} \quad (\text{A2})$$

Here, A and B are the fit parameters; B is an exponent close to 1.0. In Fig.A1, we show the Variation of $d.T_c$ with square resistance, R_{\square} , in log scale. From straight line fit, we extract $A = 1.88 \times 10^{-5}$ and $B = 0.99$. We assume that S1 and S2 also follow this scaling law with the same values of A and B . Knowing R_{\square} , then, we extract thicknesses of S1 and S2, from the straight line fit of Fig.A1, in a self-consistent way.

Method 1 and 2 provide consistent results.

Finally, we note that R_{\square} of S1 and S2 are very similar to d.c. magnetron sputtered deposited films on MgO substrate in Ref.[42] for similar thicknesses that resulted similar T_c s.

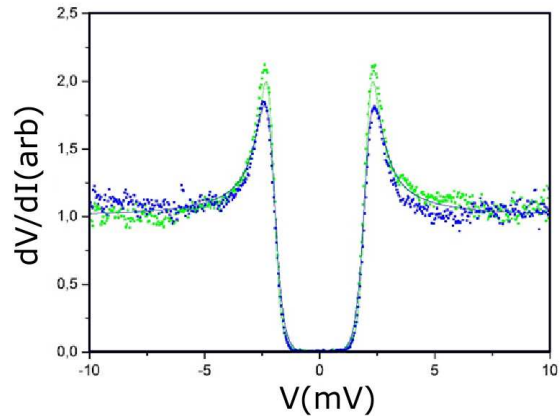


FIG. A2. Scanning tunnelling spectroscopy data at 4.2 K of a film, identical to S3, at the interior of the grain (blue) and grain boundary (green). No difference in Δ is observed.

B. f_0 as a function of temperature

We consider a resonator, side-coupled with a TL with coupling capacitance C_c , like the one shown in Fig.2b. It is well known that the resonance frequency (f_0) of such a system varies as: $f_0 \propto 1/\sqrt{L_r}$ [43], where, L_r is the inductance of the resonator. L_r has both kinetic, L_k , and geometric, L_g , component: $L_r = L_k + L_g$. Both from the measured f_0 as well as by numerical simulation using python and sonnet software, we confirm that for the three samples we have reported, L_k completely overwhelms L_g . L_k is proportional to surface inductance L_s which is given by $L_s = \mu_0 \lambda^2 / d$ for $d \ll \lambda$ [44, 45], here, μ_0 is free space permeability. The assumption, $d \ll \lambda$, is justified as $d \sim 10$ nm whereas $\lambda \sim 350$ nm. This yields Eq.2.

C. STM measurement

STM measurements are performed on a film of thickness ~ 10 nm, deposited under the identical condition of S1, S2 and S3. STS measurements at 4.2 K on the interior of the grains and grain boundaries reveal that the superconducting gap has non-noticeable variation between grain interiors and grain boundaries, confirming that there is no spatial inhomogeneity due to structural granularity. Also, no distribution of the energy gap parameter is observed. The STS spectra at higher temperatures reveal that there is no pseudogap for this film. In Fig.A2, we show two representative spectra taken at 4.2 K.

-
- [1] E. Driessen, P. Coumou, R. Tromp, P. De Visser, and T. Klapwijk, *Physical review letters* **109**, 107003 (2012).
- [2] P. W. Anderson, *Journal of Physics and Chemistry of Solids* **11**, 26 (1959).
- [3] A. Finkel'stein, *Physica B: Condensed Matter* **197**, 636 (1994).
- [4] D. Kowal and Z. Ovadyahu, *Solid state communications* **90**, 783 (1994).
- [5] A. Goldman and N. Markovic, *Phys. Today* **51**, 39 (1998).
- [6] A. Ghosal, M. Randeria, and N. Trivedi, *Physical review letters* **81**, 3940 (1998).
- [7] V. Gantmakher and M. Golubkov, *Zh. Eksp. Teor. Fiz* **109**, 1765 (1996).
- [8] A. Ghosal, M. Randeria, and N. Trivedi, *Physical Review B* **65**, 014501 (2001).
- [9] T. Baturina, A. Y. Mironov, V. Vinokur, M. Baklanov, and C. Strunk, *Physical review letters* **99**, 257003 (2007).
- [10] G. Sambandamurthy, L. Engel, A. Johansson, and D. Shahar, *Physical review letters* **92**, 107005 (2004).
- [11] G. Sambandamurthy, L. Engel, A. Johansson, E. Peled, and D. Shahar, *Physical review letters* **94**, 017003 (2005).
- [12] V. M. Vinokur, T. I. Baturina, M. V. Fistul, A. Y. Mironov, M. R. Baklanov, and C. Strunk, *Nature* **452**, 613 (2008).
- [13] S. Ghosh and S. S. Mandal, *Physical review letters* **111**, 207004 (2013).
- [14] M. Stewart, A. Yin, J. Xu, and J. M. Valles, *Science* **318**, 1273 (2007).
- [15] R. Crane, N. Armitage, A. Johansson, G. Sambandamurthy, D. Shahar, and G. Grüner, *Physical Review B* **75**, 184530 (2007).
- [16] B. Sacépé, C. Chapelier, T. Baturina, V. Vinokur, M. Baklanov, and M. Sanquer, *Physical review letters* **101**, 157006 (2008).
- [17] A. Kamlapure, T. Das, S. C. Ganguli, J. B. Parmar, S. Bhattacharyya, and P. Raychaudhuri, *Scientific reports* **3** (2013).
- [18] Y. Noat, V. Cherkez, C. Brun, T. Cren, C. Carbillat, F. Debontridder, K. Ilin, M. Siegel, A. Semenov, H.-W. Hübers, *et al.*, *Physical Review B* **88**, 014503 (2013).
- [19] A. Kamlapure, M. Mondal, M. Chand, A. Mishra, J. Jesudasan, V. Bagwe, L. Benfatto, V. Tripathi, and P. Raychaudhuri, *Applied Physics Letters* **96**, 072509 (2010).
- [20] M. Mondal, A. Kamlapure, M. Chand, G. Saraswat, S. Kumar, J. Jesudasan, L. Benfatto, V. Tripathi, and P. Raychaudhuri, *Physical review letters* **106**, 047001 (2011).
- [21] B. Sacépé, T. Dubouchet, C. Chapelier, M. Sanquer, M. Ovidia, D. Shahar, M. Feigelman, and L. Ioffe, *Nature Physics* **7**, 239 (2011).
- [22] P. Coumou, E. Driessen, J. Bueno, C. Chapelier, and T. Klapwijk, *Physical Review B* **88**, 180505 (2013).
- [23] M. Mondal, A. Kamlapure, S. C. Ganguli, J. Jesudasan, V. Bagwe, L. Benfatto, and P. Raychaudhuri, *Scientific Reports* **3** (2013).
- [24] W. Liu, M. Kim, G. Sambandamurthy, and N. Armitage, *Physical Review B* **84**, 024511 (2011).
- [25] N. Samkharadze, A. Bruno, P. Scarlino, G. Zheng, D. DiVincenzo, L. DiCarlo, and L. Vandersypen, *Physical Review Applied* **5**, 044004 (2016).
- [26] F. Luthi, T. Stavenga, O. Enzing, A. Bruno, C. Dickel, N. Langford, M. A. Rol, T. Jespersen, J. Nygard, P. Krogstrup, *et al.*, arXiv preprint arXiv:1711.07961 (2017).
- [27] A. Landig, J. Koski, P. Scarlino, U. Mendes, A. Blais, C. Reichl, W. Wegscheider, A. Wallraff, K. Ensslin, and T. Ihn, arXiv preprint arXiv:1711.01932 (2017).
- [28] N. Maleeva, L. Gruenhaupt, T. Klein, F. Levy-Bertrand, O. Dupré, M. Calvo, F. Valenti, P. Winkel, F. Friedrich, W. Wernsdorfer, *et al.*, arXiv preprint arXiv:1802.01859 (2018).
- [29] N. Samkharadze, G. Zheng, N. Kalhor, D. Brousse, A. Sammak, U. Mendes, A. Blais, G. Scappucci, and L. Vandersypen, *Science* **359**, 1123 (2018).
- [30] A. Grimm, PhD Thesis: Josephson photonics: Statistics of photons emitted by inelastic Cooper pair tunneling, Grenoble University (2015).
- [31] A. Grimm, S. Jebari, D. Hazra, F. Blanchet, F. Gustavo, J. Thomassin, and M. Hofheinz, *Superconductor Science and Technology* **30**, 105002 (2017).
- [32] P. A. Lee and T. Ramakrishnan, *Reviews of Modern Physics* **57**, 287 (1985).
- [33] M. Khalil, M. Stoutimore, F. Wellstood, and K. Osborn, *Journal of Applied Physics* **111**, 054510 (2012).
- [34] M. Tinkham, *Introduction to superconductivity*, Dover (1996).
- [35] M. Chand, PhD Thesis, Tata Institute of Fundamental Research, India (2012).
- [36] C. Aberkane, Nano-scale electronic inhomogeneities in ultra-thin superconducting NbN, Université Pierre et Marie Curie-Paris VI (2014).
- [37] R. Ganguly, D. Chaudhuri, P. Raychaudhuri, and L. Benfatto, *Physical Review B* **91**, 054514 (2015).
- [38] L. Benfatto, C. Castellani, and T. Giamarchi, *Physical review letters* **98**, 117008 (2007).
- [39] L. Benfatto, C. Castellani, and T. Giamarchi, *Physical Review B* **77**, 100506 (2008).
- [40] D. Hazra, N. Tsavdaris, A. Mukhtarova, M. Jacquemin, F. Blanchet, R. Albert, S. Jebari, A. Grimm, A. Konar, E. Blanquet, *et al.*, *Physical Review B* **97**, 144518 (2018).
- [41] Y. Ivry, C.-S. Kim, A. E. Dane, D. De Fazio, A. N. McCaughan, K. A. Sunter, Q. Zhao, and K. K. Berggren, *Physical Review B* **90**, 214515 (2014).
- [42] M. Mondal, S. Kumar, M. Chand, A. Kamlapure, G. Saraswat, G. Seibold, L. Benfatto, and P. Raychaudhuri, *Physical review letters* **107**, 217003 (2011).
- [43] D. M. Pozar, *Microwave engineering*, John Wiley & Sons (2009).
- [44] W. Henkels and C. Kircher, *IEEE Transactions on magnetics* **13**, 63 (1977).
- [45] A. Barone and G. Paterno, *Physics and applications of the Josephson effect*, Wiley Online Library **1**.